Intermetal Coupling in $[(\eta^5\text{-}C_5R_5)Fe(dppe)]_2(\mu\text{-}CH{=}CHCH{=}CH)$ and in Their Dicationic and Monocationic Mixed-Valence Forms

Min-Chul Chung,† Xinhong Gu, Beth A. Etzenhouser, Anne Marie Spuches, Peter T. Rye, Sripriya K. Seetharaman, David J. Rose, Jon Zubieta, and Michael B. Sponsler*

Department of Chemistry, Syracuse University, Syracuse, New York 13244-4100

Received February 11, 2003

The butadienediyl-bridged complexes $[(\eta^5\text{-}C_5R_5)Fe(dppe)]_2(\mu\text{-}CH{=}CHCH{=}CH)$ (R = H, Me) and their radical cationic and dicationic forms have been prepared and characterized by cyclic voltammetry, electronic spectroscopy (UV−vis and near-IR), EPR, and X-ray crystallography (R = Me). Comparisons with each other and with the literature complexes $[(\eta^5\text{-}C_5H_5)Fe(dppm)]_2(\mu\text{-}CH{=}CHCH{=}CH)$, $[(\eta^5\text{-}C_5Me_5)Fe(dppe)]_2(\mu\text{-}C{\equiv}CC{\equiv}C)$, and $[(\eta^5\text{-}C_5Me_5)\text{-}Fe(dppe)]_2(\mu\text{-}C(OMe){=}CHCH{=}C(OMe))$ have allowed for systematic evaluation of several structural variations (C_5H_5 vs C_5Me_5, dppm vs dppe, μ-CH=CHCH=CH vs μ-C≡CC≡C, and μ-CH=CHCH=CH vs μ-C(OMe)=CHCH=C(OMe)) and their effects on spectra and electronic intermetal coupling. Some of the structural changes have opposite effects on H_{ab}, the effective coupling parameter, and K_c, the comproportionation constant. The data for the mixed-valence cations are most consistent with electronic delocalization.

Many recent examples of transition metals linked with conjugated bridges have shown that such bridges can promote electronic coupling between metal centers.[1] Studies of mixed-valence (MV) ions in comparison with fully oxidized and fully reduced states have provided much insight concerning delocalization and/or intramolecular electron transfer[2] and have allowed more accurate predictions concerning potential use as molecular wires.[3] Through systematic evaluation of trends related to isolated structural variations, the role of different structural aspects has sometimes been discerned.[4] For complexes linked by conjugated hydrocarbon bridges, such systematic studies are rare.[5]

We have previously described the preparation of several butadienediyl-bridged diiron complexes, $[CpFeLL']_2(\mu\text{-}CH{=}CHCH{=}CH)$ (**1**−**4**, Cp = η^5-C_5H_5; Scheme 1), and the oxidation of these neutral species to dicationic and MV radical cationic species.[6] Lapinte and co-workers have reported the closely related butadiynediyl-bridged complex $[Cp^*Fe(dppe)]_2(\mu\text{-}C{\equiv}CC{\equiv}C)$ (**7**, Cp* = η^5-C_5Me_5, dppe = $Ph_2PCH_2CH_2PPh_2$)[7] and the butadienediyl-bridged complex $[Cp^*Fe(dppe)]_2\text{-}(\mu\text{-}C(OMe){=}CHCH{=}C(OMe))$ (**8**),[8] each also prepared in three oxidation levels. Though the MV cation forms of all of these species were found to be delocalized, class III[9] complexes, several interesting differences were

† Present address: Department of Chemical Engineering, Sunchon National University, Korea.

(1) (a) Liu, S. H.; Xia, H.; Wen, T. B.; Zhou, Z.; Jia, G. *Organometallics* **2003**, *22*, 737−743. (b) Liu, S. H.; Chen, Y.; Wan, K. L.; Wen, T. B.; Zhou, Z.; Lo, M. F.; Williams, I. D.; Jia, G. *Organometallics* **2002**, *21*, 4984−4992. (c) Enriquez, A. E.; Templeton, J. L. *Organometallics* **2002**, *21*, 852−863. (d) Rabier, A.; Lugan, N.; Mathieu, R. *J. Organomet. Chem.* **2001**, *617*−*618*, 681−695. (e) Ren, T.; Zou, G.; Alvarez, J. C. *Chem. Commun.* **2000**, 1197−1198. (f) Barigelletti, F.; Flamigni, L. *Chem. Soc. Rev.* **2000**, *29*, 1−12. (g) Hore, L.-A.; McAdam, C. J.; Kerr, J. L.; Duffy, N. W.; Robinson, B. H.; Simpson, J. *Organometallics* **2000**, *19*, 5039−5048. (h) Stein, E.; Oki, S. Y.; Vichi, E. J. S. *J. Braz. Chem. Soc.* **2000**, *11*, 252−256. (i) Alias, Y.; Abasq, M.-L.; Barrière, F.; Davies, S. C.; Fairhurst, S. A.; Hughes, D. L.; Ibrahim, S. K.; Talarmin, J.; Pickett, C. J. *Chem. Commun.* **1998**, 675−676. (j) Xia, H. P.; Yeung, R. C. Y.; Jia, G. *Organometallics* **1997**, *16*, 3557−3560. (k) Jia, G.; Wu, W. F.; Yeung, R. C. Y.; Xia, H. P. *J. Organomet. Chem.* **1997**, *539*, 53−59. (l) Hradsky, A.; Bildstein, B.; Schuler, N.; Schottenberger, H.; Jaitner, P.; Ongania, K.-H.; Wurst, K.; Launay, J.-P. *Organometallics* **1997**, *16*, 392−402. (m) Beljonne, D.; Colbert, M. C. B.; Raithby, P. R.; Friend, R. H.; Brédas, J. L. *Synth. Met.* **1996**, *81*, 179−183.

(2) (a) Le Stang, S.; Paul, F.; Lapinte, C. *Organometallics* **2000**, *19*, 1035−1043. (b) Jones, N. D.; Wolf, M. O.; Giaquinta, D. M. *Organometallics* **1997**, *16*, 1352−1354. (c) Astruc, D. *Acc. Chem. Res.* **1997**, *30*, 383−391. (d) Weyland, T.; Lapinte, C.; Frapper, G.; Calhorda, M. J.; Halet, J.-F.; Toupet, L. *Organometallics* **1997**, *16*, 2024−2031. (e) Brady, M.; Weng, W.; Zhou, Y.; Seyler, J. W.; Amoroso, A. J.; Arif, A. M.; Böhme, M.; Frenking, G.; Gladysz, J. A. *J. Am. Chem. Soc.* **1997**, *119*, 775−788. (f) Creutz, C.; Taube, H. *J. Am. Chem. Soc.* **1973**, *95*, 1086−1094.

(3) Robertson, N.; McGowan, C. A. *Chem. Soc. Rev.* **2003**, *32*, 96−103. Molecular wires composed of transition metals linked by linear carbon chains have been studied by a number of researchers. For a review, see ref 5a. For early papers, see: (a) Worth, G. H.; Robinson, B. H.; Simpson, J. *Organometallics* **1992**, *11*, 3863−3874. (b) Le Narvor, N.; Lapinte, C. *Chem. Commun.* **1993**, 357−359. (c) Zhou, Y.; Seyler, J. W.; Weng, W.; Arif, A. M.; Gladysz, J. A. *J. Am. Chem. Soc.* **1993**, *115*, 8509−8510. (d) Yam, V. W.-W.; Lau, V. C.-Y.; Cheung, K.-K. *Organometallics* **1996**, *15*, 1740−1744.

(4) (a) Launay, J.-P. *Chem. Soc. Rev.* **2001**, *30*, 386-397. (b) Ziessel, R.; Hissler, M.; El-ghayoury, A.; Harriman, A. *Coord. Chem. Rev.* **1998**, *178*−*180*, 1251−1298. (c) McCleverty, J. A.; Ward, M. D. *Acc. Chem. Res.* **1998**, *31*, 842−851. (d) Ward, M. D. *Chem. Soc. Rev.* **1995**, *24*, 121−134. (e) Crutchley, R. J. *Adv. Inorg. Chem.* **1994**, *41*, 273−325. (f) Sauvage, J.-P.; Collin, J.-P.; Chambron, J.-C.; Guillerez, S.; Coudret, C.; Balzani, V.; Barigelletti, F.; De Cola, L.; Flamigni, L. *Chem. Rev.* **1994**, *94*, 993−1019. (g) Creutz, C. *Prog. Inorg. Chem.* **1983**, *30*, 1−73. (h) Hush, N. S. *Prog. Inorg. Chem.*, **1967**, *8*, 391−444.

(5) (a) Paul, F.; Lapinte, C. *Coord. Chem. Rev.* **1998**, *178*−*180*, 431−509. (b) Dembinski, R.; Bartik, T.; Bartik, B.; Jaeger, M.; Gladysz, J. A. *J. Am. Chem. Soc.* **2000**, *122*, 810−822. (c) Frohnapfel, D. S.; Woodworth, B. E.; Thorp, H. H.; Templeton, J. L. *J. Phys. Chem. A* **1998**, *102*, 5665−5669.

(6) (a) Etzenhouser, B. A.; Chen, Q.; Sponsler, M. B. *Organometallics* **1994**, *13*, 4176−4178. (b) Etzenhouser, B. A.; Cavanaugh, M. D.; Spurgeon, H. N.; Sponsler, M. B. *J. Am. Chem. Soc.* **1994**, *116*, 2221−2222.

10.1021/om0300979 CCC: $25.00
Publication on Web 07/18/2003

Scheme 1

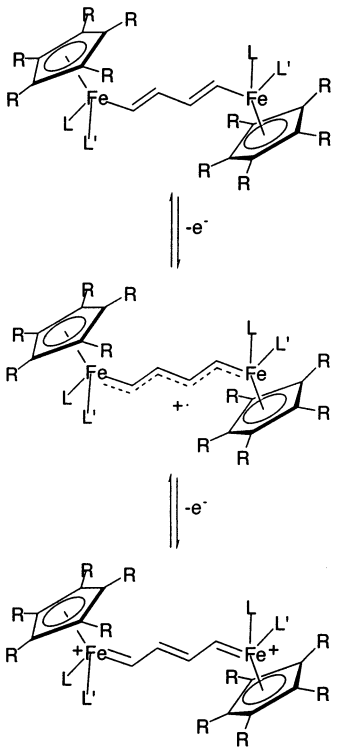

Compound	R	L, L'
1	H	2CO
2	H	CO, PMe_3
3	H	CO, PPh_3
4	H	η^2-dppm
5	H	η^2-dppe
6	CH_3	η^2-dppe

reported, such as the colors of the dications, the comproportionation constants, and the effective coupling parameters. However, since structural differences exist in both the bridge and ancillary ligands, the origin of the differences in properties between **4** and **7** and between **4** and **8** has not been clear. In this paper, we report the characterization of two intermediate structures that allow more direct and meaningful comparisons: $[(\eta^5\text{-}C_5R_5)Fe(dppe)]_2(\mu\text{-}CH{=}CHCH{=}CH)$ (R = H (**5**), Me (**6**); Scheme 1).

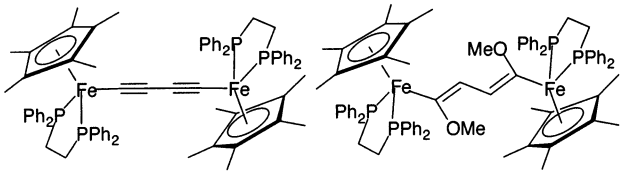

7 **8**

Results and Discussion

Synthesis of 5, 6, and Oxidized Forms. Complex **5** was prepared in a manner similar to complex **4**,[6a] by photochemical substitution of **1** with dppe. For the synthesis of **6**, the tetracarbonyl complex **9** was required, and this was prepared in a manner similar to complex **1**,[10] though with more difficulty (Scheme 2).[11] The commercial dimer, $[Cp^*Fe(CO)_2]_2$, was reduced with sodium−potassium alloy to produce the iron anion $Cp^*Fe(CO)_2K$, which was treated with *cis*-3,4-dichlorocyclobutene. When the reaction was performed at ambient temperature, complex **9** was obtained directly in a mixture with the starting dimer. When the substitution step was done at −25 °C, the diiron cyclobutene complex **10** was produced in 22% yield after recrystallization. Clean samples of complex **10** were quantitatively converted by heating to the butadienediyl complex **9**, which required no purification for subsequent reactions. Removal of $[Cp^*Fe(CO)_2]_2$ from samples of **9** proved difficult, but much of it could be removed by trituration with ether or ether/CH_2Cl_2 mixtures. Compound **6** was prepared by photochemical substitution of **9**, either pure samples prepared from **10** or samples containing some $[Cp^*Fe(CO)_2]_2$. In either case, pure **6** was obtained by recrystallization.

Scheme 2

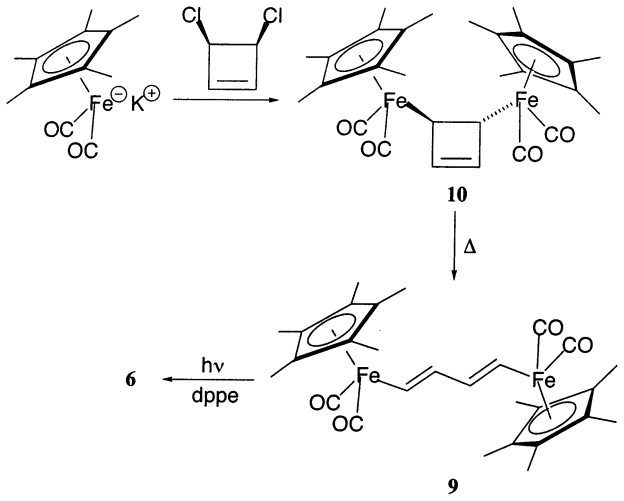

Two aspects of the nucleophilic substitution reaction of $Cp^*Fe(CO)_2K$ with *cis*-3,4-dichlorocyclobutene to form **9** or **10** deserve comment. First, unlike the analogous reaction that provides **1**, the use of the potassium salt was found to be critical. Reactions using $Cp^*Fe(CO)_2Na$ produced complicated mixtures of mono- and disubstituted products in both open and closed forms. Temperature was also a critical determinant of the outcome.

The observation of **9** as the room-temperature product is very interesting, given that the **10** formed at low temperature survives even after the reaction mixture is warmed to room temperature.[12] (The thermal conversion of **10** to **9** requires several days at room temperature.) This has interesting mechanistic implications that might be elucidated with further experiments. It must be that **10** is not an intermediate in the room-temperature reaction (i.e., the mechanism is strongly temperature dependent), the **10** formed undergoes a chemically activated ring opening to produce **9**, or the **10** formed is sensitive to minor impurities that arise only at room temperature. A similar observation was made in the Cp version of the reaction,[10] but the mechanistic implications were not mentioned.

(7) (a) Le Narvor, N.; Toupet, L.; Lapinte, C. *J. Am. Chem. Soc.* **1995**, *117*, 7129−7138. (b) Coat, F.; Thominot, P.; Lapinte, C. *J. Organomet. Chem.* **2001**, *629*, 39−43. (c) For the complex analogous to **7** with $i\text{Pr}_2\text{-PCH}_2\text{CH}_2\text{P}i\text{Pr}_2$ ligands, see: Guillemot, M.; Toupet, L.; Lapinte, C. *Organometallics* **1998**, *17*, 1928−1930.

(8) Guillaume, V.; Mahias, V.; Mari, A.; Lapinte, C. *Organometallics* **2000**, *19*, 1422−1426.

(9) Robin, M. B.; Day, P. *Adv. Inorg. Chem. Radiochem.* **1967**, *10*, 247−422.

(10) (a) Sanders, A.; Giering, W. P. *J. Organomet. Chem.* **1976**, *104*, 67−78. (b) Sanders, A.; Giering, W. P. *J. Am. Chem. Soc.* **1974**, *96*, 5247−5248.

(11) (a) Etzenhouser, B. A. Ph.D. Dissertation, Syracuse University, Dec 1995. (b) Gu, X. Ph.D. Dissertation, Syracuse University, Dec 1997.

(12) The low-temperature reaction to form **10** was only started at low temperature and then the mixture was warmed to room temperature.

Table 1. Electrochemical Potentials and Comproportionation Constants[a] for $(C_5R_5)L_2Fe-R'-FeL_2(C_5R_5)$ or $(C_5R_5)L_2Fe-R'$

compd	R	L_2	R′	E_1 (V)	E_2 (V)	ΔE (mV)	K_c
4[b]	H	dppm	μ-C_4H_4	−1.17	−0.73	440	2.9×10^7
5[c]	H	dppe	μ-C_4H_4	−1.17	−0.70	470	9.2×10^7
6[c]	Me	dppe	μ-C_4H_4	−1.25	−0.65	600	1.5×10^{10}
7[d]	Me	dppe	μ-C_4	−1.09	−0.38	710	1.1×10^{12}
8[e]	Me	dppe	μ-$C_4H_2(OMe)_2$	−1.50	−1.07	430	1.9×10^7
mono Fe[e,f]	Me	dppe	CH=CH_2	−0.78			
	Me	dppe	CH=CHCH=CH_2	−0.80			
	Me	dppe	C≡CH	−0.57			
	Me	dppe	C≡CC≡CH	−0.44			
	Me	dppe	C(OMe)=CH_2	−0.81			

[a] All measurements were made at room temperature in CH_2Cl_2 with $n$$Bu_4NPF_6$ as electrolyte. Potentials are referenced to $Cp_2Fe^{0/+}$. [b] Reference 6a. [c] This work. [d] Reference 7. [e] Reference 5a. [f] The monoiron complexes listed all display waves that are not fully reversible (i_a/i_c = 0.5 to 0.8), but the resulting approximation in these E_1 values should be small relative to the comparisons cited in the text.

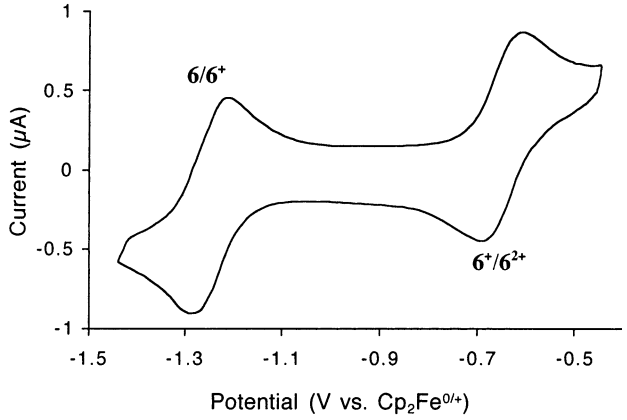

Figure 1. Cyclic voltammogram of **6** (5×10^{-4} M in 0.1 M Bu_4NPF_6 in CH_2Cl_2, referenced to $Cp_2Fe^{0/+}$ at 0.0 V, room temperature, 50 mV/s).

Oxidation of **5** and **6** was accomplished either electrochemically or chemically. Each complex exhibited two reversible oxidation waves by cyclic voltammetry (CV) at the potentials listed in Table 1. Controlled-potential electrolysis provided solutions of the oxidized species and confirmed that each wave represents a single-electron oxidation. Chemical oxidation was done with either silver tetrafluoroborate ($AgBF_4$) or ferrocenium hexafluorophosphate ($FcPF_6$). Treatment of **5** with excess $AgBF_4$ or stoichiometric $FcPF_6$ produced the purple **5[BF4]2** or **5[PF6]2**, respectively, which were found to be air-stable in both the solution and solid phases. Comproportionation of **5** and either $\mathbf{5}^{2+}$ salt produced salts of $\mathbf{5}^{+}$, as expected from the high comproportionation constant (Table 1). The purple MV cation $\mathbf{5}^{+}$ was found to be air-sensitive but persistent on a time scale of hours under nitrogen at room temperature. Treatment of **6** with excess $AgBF_4$ led to impure samples of **6[BF4]2**, apparently due to overoxidation.[13] However, the use of 2 equiv of $FcPF_6$ gave **6[PF6]2** cleanly. The deep blue dication $\mathbf{6}^{2+}$ was stable under nitrogen at room temperature, but solutions exposed to air turned pale yellow over several hours. The pink **6[PF6]** was prepared either by comproportionation of **6** and **6[PF6]2** or by oxidation of **6** with 1 equiv of $FcPF_6$. The stability of **6[PF6]** was similar to that of **5[PF6]**.

For the oxidized forms of compound **4**, both BF_4^- and PF_6^- salts were studied spectroscopically, and differences in the spectral data were found to be insignificant. In the remainder of this paper, the counterion is PF_6^- when not specified.

Cyclic Voltammetry and Comproportionation Constants (K_c). Complexes **4**−**8** all show two well-resolved, single-electron, reversible oxidation waves by CV, and a representative voltammogram is shown for complex **6** in Figure 1. Table 1 shows the comproportionation constants (K_c, the equilibrium constant for the comproportionation equilibrium; eq 1) calculated from

$$A + A^{2+} \overset{K_c}{\rightleftharpoons} 2A^{+} \qquad (1)$$

the CV data[4g] for **4**−**8**. The K_c values are all very high, ranging from 10^7 to 10^{12}. The comparison between **6** and **7** shows that the acetylenic bridge gives a K_c value 70 times higher than does the olefinic bridge. Table 1 also shows that replacing dppm with dppe (comparing **4** and **5**) increases K_c by a factor of 3, replacing Cp with Cp* (comparing **5** and **6**) increases K_c by a factor of 160, and replacing α-hydrogens on the bridge with methoxy substituents (comparing **6** and **8**) decreases K_c by a factor of 800.

Comproportionation constants are very commonly cited to show electronic delocalization in MV compounds.[14] Electronic delocalization tends to stabilize a MV complex and therefore increase K_c (see eq 1). The K_c values for **4**−**8** given in Table 1 are all very high and support the idea that the MV forms of all of these complexes enjoy considerable stabilization due to delocalization.

Other phenomena besides delocalization also contribute to K_c,[15] and one must therefore be careful in interpreting the meaning of K_c trends. For example, Coulombic repulsion between charges destabilizes the dication and increases K_c. Solvation of these charges and ion pairing reduce this effect and therefore decrease K_c.[16] Solvation of the monocations may also be important but is generally less so, especially if the charge is delocalized. Thus, steric hindrance of solvation and ion pairing by the Cp* methyl groups might serve to destabilize $\mathbf{6}^{2+}$, helping to explain the higher K_c value for **6** relative to that for **5**. In $\mathbf{8}^{2+}$, the expanded π system that includes the methoxy oxygens presumably results in a decreased Coulombic repulsion between the charges,

(13) Oxidation to a trication was reported for an analogue of $\mathbf{7}^{2+}$.[7c]

(14) See, for example, refs 1−5.

(15) (a) Evans, D. H.; Lehmann, M. W. *Acta Chem. Scand.* **1999**, *53*, 765−774. (b) Richardson, D. E.; Taube, H. *J. Am. Chem. Soc.* **1983**, *105*, 40−51.

contributing to the lower K_c value for **8** relative to that for **6**. Other factors that affect the thermodynamics include stabilization of the dication through extra π bond formation or antiferromagnetic coupling, differences in bridge binding energies between the oxidation states (a related effect), and entropic effects (both internal and solvation).

Additional insight concerning stabilization/destabilization effects can be gained by considering the absolute redox potentials, not just their difference that leads to K_c. For this purpose, comparison of both the first and second oxidation potentials (E_1 and E_2) to the oxidation potential of a mononuclear model complex is useful. Indeed, in the case where the two metal centers are isolated from each other (noncoupled), E_1 and E_2 would be expected to be not only the same as each other but also very close to the oxidation potential for a mononuclear model with similar structure. In this sense, two molecules of the mononuclear complex may be taken as analogous to a noncoupled version of the dinuclear complex, allowing an analysis of relative stabilization/destabilization effects that arise due to coupling in the dinuclear complexes.

Fortunately, electrochemical data are available from Lapinte's work for appropriate mononuclear models for complexes **6**−**8**, and these data are included in Table 1. In some cases, the best choice of model is unclear—whether one should select a model that includes half of the bridging ligand or all of it. While both types of models are shown in Table 1, for consistency we have used the "half-bridge" models in the comparisons below simply because more of these are available. The arguments would be qualitatively unchanged with the other choice of models.

The first oxidation potentials of **6**−**8** are 0.5−0.7 V more negative than the oxidation potentials of the corresponding mononuclear models, indicating that the MV cations are significantly stabilized by coupling (or, less likely, that the neutral complexes are destabilized by coupling). The oxidation potentials of $\mathbf{6}^+$ and $\mathbf{7}^+$ (E_2) are 0.1−0.2 V more positive than the oxidation potentials of the mononuclear cations, consistent with a destabilization of the dications by Coulombic repulsion.

Interestingly, the oxidation potential of $\mathbf{8}^+$ is 0.26 V more negative than that of the model, indicating a coupling *stabilization* of $\mathbf{8}^{2+}$ despite Coulombic repulsion. Also striking is the very large, 0.69 V stabilization

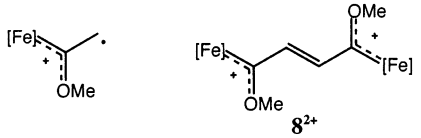

$\mathbf{8}^{2+}$

of $\mathbf{8}^+$ due to coupling. Insight might be drawn from structures such as the ones shown above. Clearly, $\mathbf{8}^{2+}$ enjoys the resonance stabilization of Fischer carbenes, while similar stabilization in the mononuclear cation is attenuated by the necessity of placing the unpaired electron on carbon. Another possible explanation is that strain involving the methoxy groups is relieved by twisting around bridge bonds as the complex is oxidized.[17] This explanation is also consistent with the lower near-IR extinction coefficient observed for $\mathbf{8}^+$ (Table 2).

Table 2. Near-IR Bands and Effective Coupling Parameters (H_{ab})

compd	λ_{max} (nm)	ϵ_{max} (cm^{-1} M^{-1})	ν_{max} (cm^{-1})	$\Delta\nu$ (cm^{-1})	$\Delta\nu$ (Hush, cm^{-1})[a]	H_{ab} (eV)[b]
$\mathbf{4}^{+c}$	1296	8000[d]	7716	2380	4222	0.48
$\mathbf{5}^{+e}$	1269	10000	7880	2967	4266	0.49
$\mathbf{6}^{+e}$	1427	14000	7008	5047	4023	0.43
$\mathbf{7}^{+f}$	1326	11700	7541	3250	4174	0.47
$\mathbf{8}^{+g}$	1150	3350	8696	3996	4482	0.54

[a] Calculated as described in ref 4g,h. [b] Calculated for class III complexes; $H_{ab} = \nu_{max}/2$. [c] Reference 6a. [d] This value has been corrected slightly from the value in ref 6a. [e] This work. [f] Reference 7. [g] Reference 5a.

Comparing potentials for the dinuclear complexes reveals several notable trends. Replacing the H's on Cp with methyl groups (**5** → **6**) leads to an easier first oxidation (more negative E_1 by 0.08 V), presumably due to electron donation from the methyls. However, the second oxidation is less favorable (more positive E_2 by 0.05 V), perhaps due to the hindrance of solvation and ion pairing noted above. The increased ΔE (either or both of the potential shifts) might be attributed also to increased stabilization of the cation through delocalization, but H_{ab} values do not support this (see below). Replacing H's on the bridge with methoxy groups (**6** → **8**) leads to a 0.25 V more favorable first oxidation, a remarkable point, given that the same substitution in the mononuclear complexes leads to almost no change. The methoxy groups lead to an even more favorable second oxidation (by 0.42 V). These arguments suggest, and are corroborated by near-IR data discussed below, that the relatively low ΔE and K_c values for **8** are caused by a stabilization of $\mathbf{8}^{2+}$ and not by a relative destabilization of $\mathbf{8}^+$.

The trend between **6** and **7** roughly follows the trend from the mononuclear complexes, but further interpretation is difficult. The slightly smaller ΔE value for **6** may include contributions from a stabilization of $\mathbf{6}^{2+}$ due to minor charge delocalization to the bridge H's and an entropic stabilization of $\mathbf{7}^+$ relating to the presence of two bridge π systems. Therefore, the observed trend in oxidation potentials, though suggestive of greater stabilization in $\mathbf{7}^+$, is inconclusive with regard to the relative role of electronic delocalization in $\mathbf{6}^+$ and $\mathbf{7}^+$.

Near-IR Spectroscopy. Like $\mathbf{4}^+$, $\mathbf{7}^+$, and $\mathbf{8}^+$, the MV radical cations $\mathbf{5}^+$ and $\mathbf{6}^+$ each show strong absorptions in the near-IR that are absent in the spectra of the neutral and dicationic complexes (Figure 2 and Table 2). These bands are more readily assigned as MV $\pi-\pi$ bands[18] of delocalized complexes (Robin and Day class III[9]) than as intervalence transfer (IT) bands of localized (class II) ions. While Meyer's designation of class II/III (electronically localized but solvent averaged due to rapid electron transfer)[19] cannot be ruled out on the basis of the data reported herein, these complexes are clearly strongly coupled. IR spectra for $\mathbf{3}^+$ [6b] and its Cp*

(16) Solvation and ion-pairing effects can be very large: Barrière, F.; Camire, N.; Geiger, W. E.; Mueller-Westerhoff, U. T.; Sanders, R. *J. Am. Chem. Soc.* **2002**, *124*, 7262−7263.

(17) A similar argument for various redox compounds appears in ref 15a.

(18) In these complexes, both π orbitals are expected to be bonding orbitals, though antibonding with respect to the Fe−C bonds. See Figure 3.

(19) Demadis, K. D.; Hartshorn, C. M.; Meyer, T. J. *Chem. Rev.* **2001**, *101*, 2655−2685.

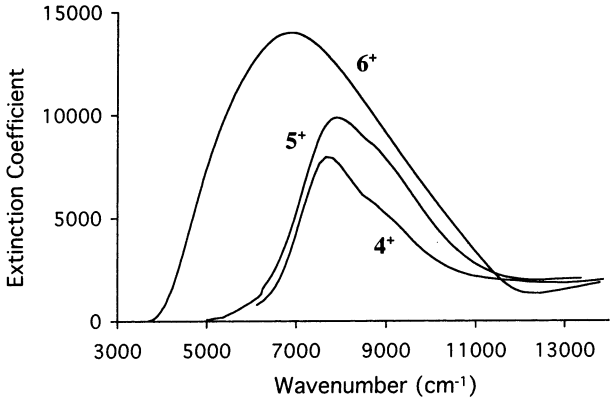

Figure 2. Near-IR spectra of $\mathbf{4}^+$, $\mathbf{5}^+$, and $\mathbf{6}^+$ in CH_2Cl_2 at room temperature.

analogue[20] each show a single CO stretch, indicating that these related complexes are delocalized on the vibrational time scale.

Solvent independence of λ_{max} over a wide range of solvent polarity is a clear indication of the averaged solvation of either a delocalized (III) or very rapidly equilibrating (II/III) ion. Complex $\mathbf{4}^+$ shows maxima of 1298, 1297, and 1295 nm in CH_2Cl_2, acetone, and acetonitrile, respectively, while complex $\mathbf{6}^+$ shows maxima of 1427, 1420, 1425, and 1420 nm in CH_2Cl_2, acetone, methanol, and acetonitrile, respectively.

Class III and II/III ions generally exhibit narrower MV bands: in particular, markedly narrower than the widths predicted by Hush theory.[4g,19,21] Narrow bands by this measure are indeed observed for all but one of the ions $\mathbf{4}^+$–$\mathbf{8}^+$ (Table 2). The band for $\mathbf{6}^+$ is considerably broader than the bands for the other ions. The width of this peak actually exceeds the prediction from Hush theory.

The near-IR band shapes for $\mathbf{4}^+$ and $\mathbf{5}^+$ are characteristic for class III or II/III complexes,[19,22] showing a relatively sharp cutoff on the low-energy side and apparent shoulders on the high-energy side that might represent vibrational progressions[23] (if class III) or unresolved subbands (if either class III or II/III).[19] For $\mathbf{6}^+$, the low-energy cutoff is apparent, but high-energy shoulders are not. A possible explanation is that the progression or subbands in this case are stronger but not resolved, leading to the large apparent width.

Whether the complexes are class III or II/III, the low-energy cutoff occurs at $2H_{ab}$,[22] where H_{ab} is the effective coupling parameter. Taking the cutoff value as the peak maximum, the H_{ab} values in Table 2 are obtained. For a class III species, the method for finding H_{ab} is the same: taking the peak maximum as $2H_{ab}$. For a class II or II/III species, H_{ab} can be found from the IT band by using eq 2, where H_{ab}, $\bar{\nu}_{max}$, and $\bar{\nu}$ are in cm^{-1}, ϵ is in $M^{-1}\,cm^{-1}$, and d is the electron-transfer distance in Å.[19] Assuming that the entire near-IR bands represent the lowest energy IT band and taking d as the Fe–Fe distance in **6** of 7.549 Å (Table 5), values of H_{ab} were obtained that were 2–3 times lower than the values in Table 2 (from 0.14 eV for $\mathbf{4}^+$ to 0.23 eV for $\mathbf{6}^+$). Equation 2 is known to give values that are low by 2 times or possibly more,[22] but the discrepancy is presumably even larger than 2–3 times in this case. Only the lowest energy IT band should be included in the calculation with eq 2, but area from unresolved subbands was included in our calculation.[24] Partly on the basis of this discrepancy, but also in consideration of the IR data for the closely related CO complexes (see above) and the high H_{ab} values, we conclude that the near-IR bands are more consistently assigned as MV π–π bands of class III ions.

$$H_{ab}^2 = [(4.2 \times 10^{-4})\bar{\nu}_{max} \int \epsilon(\bar{\nu})\, d\bar{\nu}]/d^2 \qquad (2)$$

The H_{ab} values (Table 2) are all in a similar, high range for $\mathbf{4}^+$–$\mathbf{8}^+$. The trends in H_{ab} are in the same direction as the K_c trends in some cases but are opposite in other cases. The bridge comparison between $\mathbf{6}^+$ and $\mathbf{7}^+$ shows the same trend for H_{ab} as observed for K_c, with a higher coupling attributed to the acetylenic bridge. Replacing Cp in $\mathbf{5}^+$ with Cp* in $\mathbf{6}^+$ shows a decrease in H_{ab}, despite the increase noted in K_c. The methoxy groups of $\mathbf{8}^+$ induce a large increase in H_{ab} relative to $\mathbf{6}^+$, while a large decrease in K_c was noted above. Replacing dppm in $\mathbf{4}^+$ with dppe in $\mathbf{5}^+$ leads to small increases in both H_{ab} and K_c.

The nature of the MV π–π transitions is explored with the help of the MO mixing diagram in Figure 3, with relative fragment energies based upon DFT results for an analogue of **5** (with H replacing the phosphine Ph groups).[25] These relative energies, which are similar to related ones obtained through Fenske–Hall calculations,[26] suggest that the strongest π mixing between metal and bridging ligand will involve the HOMO of butadiene and the d_π orbital combination of correct symmetry (A), forming two π orbitals: the HOMO of the complex and a lower energy π orbital. The d_π combination of S symmetry may mix with the LUMO of butadiene, but the mixing with the lower π bonding orbital might be even more important; in any case, these mixings are not as strong. The MV π–π band is identified in Figure 3 in the usual way: from one d_π combination (S) to the other (A), though transitions from other t_{2g} orbitals could account for other subbands.

UV–Vis Spectroscopy. In general, the neutral complexes **4**–**7** are orange in the solid state and pale yellow in dilute solution, exhibiting no maxima in the visible region, with the color attributable to tails or shoulders extending from the UV (Figure 4a and Table 3).[27] The exception to this is compound **6**, which is purple-red in the solid state and red-brown in solution. This coloration is due to a strong band at 471 nm, which is unlike any band present in the other complexes.

This 471 nm band of **6** might correspond to strong bands in the other complexes that appear in the UV

(20) Chung, M. C.; Londergan, C. H.; Kubiak, C. P.; Englich, U.; Ruhlandt-Senge, K.; Etzenhouser, B. A.; Sponsler, M. B. Work in progress.
(21) Brunschwig, B. S.; Creutz, C.; Sutin, N. *Chem. Soc. Rev.* **2002**, *31*, 168–184.
(22) (a) Nelson, S. F. *Chem. Eur. J.* **2000**, *6*, 581–588. (b) Lambert, C.; Noll, G. *J. Am. Chem. Soc.* **1999**, *121*, 8434–8442.
(23) Taking the difference between the peak and the shoulder in $\mathbf{4}^+$, the complex with the most resolved band, gives a vibrational spacing of 1400 ± 100 cm^{-1}, consistent with a bridge C=C stretch.
(24) Other possible sources of error exist with respect to eq 2. The electron-transfer distance may be less than the Fe–Fe distance, and the equation is derived from an approximate two-state model.[22a]
(25) Freedman, T. B.; Sponsler, M. B. Work in progress.
(26) Sponsler, M. B. *Organometallics* **1995**, *14*, 1920–1927.
(27) UV–vis spectra have not been reported for **8** or its oxidized forms.

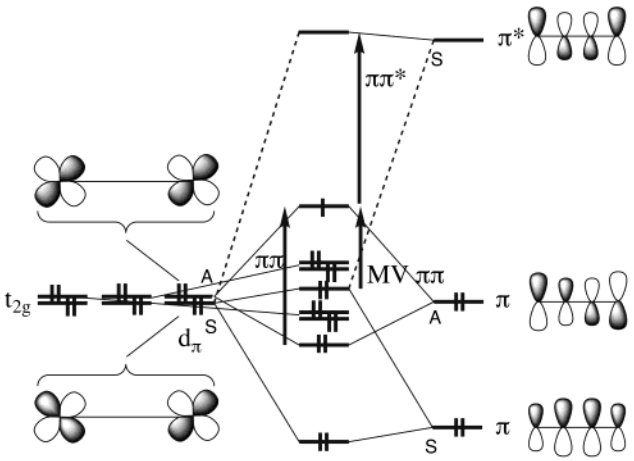

Figure 3. MO mixing diagram for **4**, **5**, or **6**. Symmetry labels are given with respect to the C_2 axis, which is parallel to the p orbitals of the bridge. Three electronic transitions are assigned on the diagram: the MV $\pi-\pi$ band, appearing in the near-IR region for the cationic complexes, the $\pi-\pi$ band, appearing in the visible region for the cationic and dicationic complexes, and the $\pi-\pi^*$ band, appearing in the visible region for the neutral complexes. Mixing partners are not shown for four of the t_{2g} orbitals, though some mixing is expected such that their energies will move up or down. The electron occupation shown is that of the cationic complexes.

region, but the red shift of **6** relative to **5** is much larger than would be expected for a simple electron donation from the methyl groups that serves to increase the energy of the HOMO. The oxidation potentials of **5** and **6** differ by only 0.08 V, suggesting that the HOMO of **6** is higher by roughly 0.08 eV, while a red shift of the absorption of **5** at 330 nm to 471 nm for **6** represents a change of 1.1 eV. A reason for a major change in the LUMO is not obvious, though the complex is clearly strained by the bulky Cp* and dppe ligands, as shown by the very large Fe−C═C angle of approximately 140°. For comparison, the analogous angle in **1** is 132°[28] and in $\mathbf{4}^{2+}$ is 129°.[6a] Nonetheless, a major change in the energy of the LUMO when none is readily apparent in the HOMO, as judged by oxidation potentials, seems doubtful.

A more likely explanation for the strong 471 nm band in **6** is that it corresponds to weak shoulders or tails in **4** and **5** in the region around 400−500 nm.[29] These bands may be assigned as $\pi-\pi^*$ bands between the HOMO and LUMO (see Figure 3). The extinction coefficient of **6** is approximately 10 times larger than that for **5** at 471 nm, a quite large effect. Again, donation from the methyl groups would not likely produce such a striking effect, but a conformational change caused by steric strain from the methyl groups is a possibility.

Insight can be gained by considering what is known about conformational effects in 1,3-butadiene. The s-trans form has an extinction coefficient approximately 2.2 times higher than that of the s-cis form,[30] though

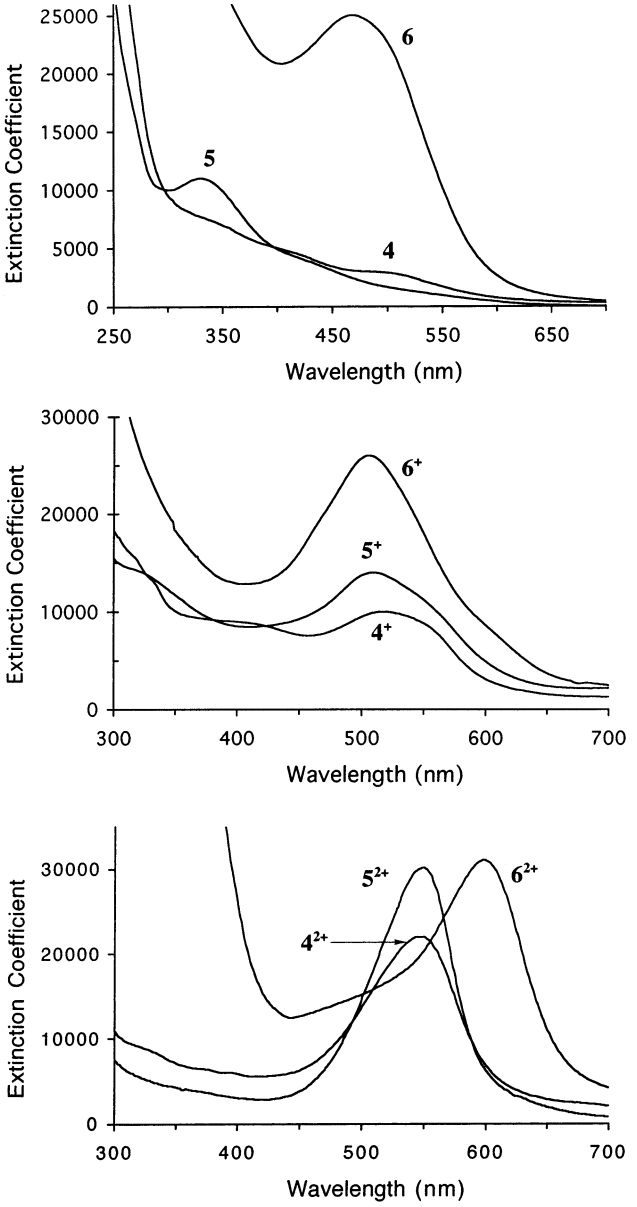

Figure 4. UV−vis spectra in CH_2Cl_2 at room temperature: (a, top) **4**, **5**, and **6**; (b, middle) $\mathbf{4}^+$, $\mathbf{5}^+$, and $\mathbf{6}^+$; (c, bottom) $\mathbf{4}^{2+}$, $\mathbf{5}^{2+}$, and $\mathbf{6}^{2+}$.

Table 3. UV−Vis Spectra

	λ_{max} (nm)			ϵ_{max} (cm^{-1} M^{-1})		
compd	neutral	cation	dication	neutral	cation	dication
4[a]	480 (sh)	518	546	3 000	10 000	30 000
5[b]	330	509	546	11 000	14 000	22 000
6[b]	471	505	597	25 000	26 000	31 000
7[c]		437	621		4 100	24 100
		567			702	

[a] Reference 6a and this work. [b] This work. [c] Reference 7.

controversy remains as to whether the s-cis form is planar or gauche.[31] While we have no information about the conformational preferences of compound **5**, the X-ray crystal structure of **6** (Figure 6, see below) shows an s-trans geometry. That a sterically encumbered complex

(28) Churchill, M. R.; Wormald, J. *Inorg. Chem.* **1969**, *8*, 1936−1941. A different crystal structure puts the angle at 126°: Davis, R. E. *Chem. Commun.* **1968**, 1218−1219.

(29) The UV−vis spectrum of **7**, as recorded by us, shows a similar tailing absorption in the visible region, but without perceptible shoulders.

(30) Squillacote, M. E.; Sheridan, R. S.; Chapman, O. L.; Anet, F. A. L. *J. Am. Chem. Soc.* **1979**, *101*, 3657−3659.

(31) Saltiel, J.; Sears, D. F., Jr.; Turek, A. M. *J. Phys. Chem. A* **2001**, *105*, 7569−7578.

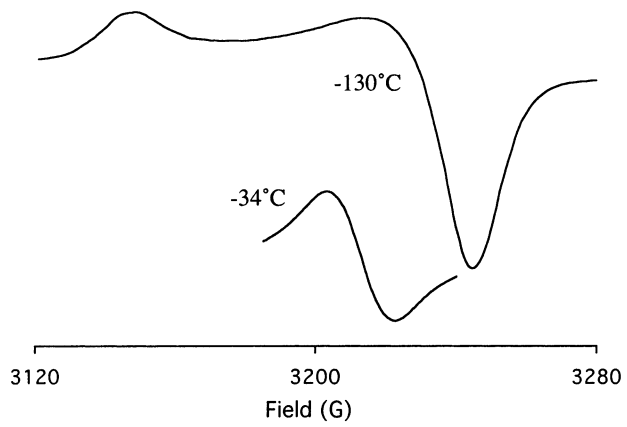

Figure 5. EPR spectra of $\mathbf{6}^+$ in CH_2Cl_2 solution (−34 °C) and frozen solution (−130 °C).

would favor s-trans is reasonable, since this gives the greatest Fe−Fe separation. Two other X-ray crystal structures[20] are suggestive that less hindered complexes such as **4** and **5** might exist at least partially in conformations other than s-trans: the structure for **3** (*dl*) shows a gauche geometry (C=C−C=C dihedral angle of 47°), while the Cp* analogue (*dl*) shows an s-trans conformation (C=C−C=C dihedral angle of 176°). Therefore, one possibility is that **4** and **5** exist as mixtures of conformations, leading to a weaker and spread-out $\pi-\pi^*$ absorption that is not well-resolved from the tail from the UV absorption, while **6** exists exclusively as the s-trans conformer, giving a well-defined and strong band.[32]

The cations $\mathbf{4}^+-\mathbf{7}^+$ are all relatively similar in their UV−vis spectra, showing strong bands from 437 to 518 nm (Figure 4b and Table 3). The high extinction coefficients suggest that these bands are $\pi-\pi$ transitions, as shown in Figure 3, though contribution from a $\pi-\pi^*$ transition analogous to that of the neutral complexes is also possible. A small solvent dependence was observed in the spectra of $\mathbf{6}^+$, which showed visible maxima at 505, 515, 514, and 500 nm in CH_2Cl_2, acetone, methanol, and acetonitrile, respectively.

The analogous $\pi-\pi$ transitions are also observed in the dications $\mathbf{4}^{2+}-\mathbf{7}^{2+}$, ranging from 546 to 621 nm (Figure 4c and Table 3). These bands are red-shifted and stronger than those in the cations. Since the upper orbital is completely empty, a higher probability of transition is expected. The red-shifted bands for $\mathbf{6}^{2+}$ and $\mathbf{7}^{2+}$ account for the blue color of these ions, in contrast to the purple $\mathbf{4}^{2+}$ and $\mathbf{5}^{2+}$.

EPR Spectroscopy. Both solution and frozen-solution EPR spectra were recorded for complexes $\mathbf{4}^+-\mathbf{6}^+$. Representative spectra for $\mathbf{6}^+$ are shown in Figure 5, and the data for $\mathbf{4}^+-\mathbf{6}^+$ are given in Table 4 along with literature data for $\mathbf{7}^+$ and $\mathbf{8}^+$. None of the cations $\mathbf{4}^+-\mathbf{6}^+$ exhibit resolved hyperfine splitting due to either ^{31}P or ^1H, even though both types of splitting were observed for $\mathbf{2}^+$ and $\mathbf{3}^+$, which allowed us to conclude that the unpaired electron is delocalized on the EPR time scale for these ions.[6b] Presuming $\mathbf{4}^+-\mathbf{6}^+$ to be also delocalized and symmetric, upper limits can be placed on the hyperfine coupling constants for any unresolved splitting. For $\mathbf{4}^+$ and $\mathbf{5}^+$, the limit for a_P, assuming coupling to four equivalent P atoms, is about 3 G. For $\mathbf{6}^+$, the observed line width was higher, and a_P is at most 9 G. The a_P values observed for $\mathbf{2}^+$ and $\mathbf{3}^+$ were 7−8 G.

(32) Our use of crystal structures to propose conformational effects in solution is admittedly speculative.

Table 4. EPR Spectra

compd	*g*, isotropic (temp, °C)	line width, peak-to-peak (G)	g, frozen soln (temp, °C)	line width, peak-to-peak (G)
$\mathbf{4}^{+a}$	2.035 (−16)	7	2.086, 2.024, 1.995 (−128)	17
$\mathbf{5}^{+b}$	2.034 (−20)	8	2.063, 2.030, 2.011 (−127)	13
$\mathbf{6}^{+b}$	2.059 (−34)	20	2.101 (∥), 2.038 (⊥) (−130)	30
$\mathbf{7}^{+c}$	2.102 (−196)		2.139, 2.089, 2.079 (−196)	
$\mathbf{8}^{+d}$	2.025 (−15)			

[a] Reference 6a. [b] This work. [c] Reference 2a. [d] Reference 5a.

Table 5. Selected Distance (Å) and Angle (deg) Data for 6[a]

Fe−C1	1.983(9), 1.989(9)
C1−C2	1.341(14), 1.349(13)
Fe−Cp*[b]	1.75(1), 1.75(1)
Fe−P	2.151(3), 2.160(3), 2.145(3), 2.156(3)
C2−C3	1.465(14)
Fe- - -Fe	7.549(2)
Fe−C1−C2	140.2(8), 138.3(8)
P−Fe−P	85.56(11), 86.63(12)
C1−C2−C3	125.4(10), 126.3(9)
C1−Fe−P	83.9(3), 90.0(3), 81.9(3), 90.3(3)
Cp*−Fe−C1−C2	143.1(4), 140.5(4)
C1−C2−C3−C4	178.7(9)

[a] Analogous bond distances and angles are listed together. [b] Cp* represents the centroid of the C_5 ring.

Lapinte and co-workers have suggested that the anisotropy of the solid-state EPR signal (Δg) is an indicator of the efficiency of a bridge for conveying electrons between Cp*Fe(dppe) centers, with greater efficiency being associated with smaller Δg values.[2a] For $\mathbf{6}^+$ and $\mathbf{7}^+$, the Δg values are very similar (though recorded at different temperatures), 0.063 and 0.060, respectively, supporting the conclusion that these complexes are very comparable in their extent of intermetal coupling. The difference, if significant, lies in the same direction as the H_{ab} and K_c trends.

X-ray Crystallography of 6. Like many of the diiron complexes, **6** crystallizes as very thin plates. However, after multiple recrystallizations and crystal mountings, a crystal that diffracted with sufficient intensity for structure refinement was found. Selected distances and angles are shown in Table 5, crystallographic data are given in Table 6, and a view of the structure is provided in Figure 6. Crystal structures of $\mathbf{4}^{2+}$ [6a] and $\mathbf{7}^+$ [7a] can be found in the literature.

The X-ray structure of **6** offers a few insights related to intermetal coupling. Mentioned above are the observations of an s-trans conformation and a very large Fe−C−C angle (138−140°), the latter showing that the complex is strained by steric crowding. The crowding may also be observed in the meshed arrangement of ligands and the short nonbonded contacts between Ph groups and opposing Cp* and ethano groups. The shortest contacts are between the bridge β-H atoms and a P on the adjacent Fe center (2.8 Å) and one H on each

Table 6. Crystallographic Data for 6

formula	$C_{91}H_{118}Fe_2P_4$
fw	1447.52
T, K	293(2)
cryst syst	triclinic
space group	$P\bar{1}$
a, Å	12.4156(3)
b, Å	16.0538(4)
c, Å	19.3644(5)
α, deg	76.950(1)
β, deg	80.801(1)
γ, deg	78.396(1)
Z	2
V, Å^3	3656.6(2)
d_{calcd}, g/cm^3	1.315
R indices, $I > 2\sigma(I)$: R1, wR2	0.0762, 0.1036

dppe ethano bridge with an opposing Ph H atom (2.4 Å). The latter is approximately twice the van der Waals radius for H.

General Comments. Many of the structural comparisons can be understood in terms of electron density effects. Electron density at Fe is approximately unchanged by replacing dppm with dppe (**4** → **5**)[33] but is increased by replacing Cp with Cp* (**5** → **6**). The methoxy groups of **8**, though inductively withdrawing, are strongly donating through resonance. The differences between **6** and **7** are also partly attributable to electron density effects, the alkynyl ligand being significantly more electron withdrawing. All of these electron density effects are observable in the E_1 values of Table 1.

The MO analysis of Figure 3 serves to identify several issues that are important with respect to comparisons of $\mathbf{6}^+$ with $\mathbf{7}^+$ and $\mathbf{8}^+$. Three factors are expected to be important for $\mathbf{7}^+$: (1) the presence of a second π system that can mix with the orthogonal set of d_π orbitals, (2) the considerably wider $\pi-\pi^*$ gap in the bridging ligand, and (3) the considerably stronger electronegativity of the alkynyl ligand. The electronegativity will serve to lower the d_π orbital energies, an effect that balances against the lower energy of the butadiyne π orbital. Another issue that may be important is that conformational nonplanarity may attenuate orbital overlap and electronic coupling in $\mathbf{6}^+$ but not in $\mathbf{7}^+$, although we have argued above that the s-trans conformation may be strongly favored even in the neutral **6** due to steric interactions. The incorporation of bridge methoxy groups in $\mathbf{8}^+$ introduces two new bridge π-symmetry orbitals that will be energetically fairly close to the d_π orbitals, potentially changing the bonding picture quite significantly.

Very interesting questions remain concerning the magnetic properties of the dications $\mathbf{5}^{2+}$ and $\mathbf{6}^{2+}$, since $\mathbf{4}^{2+}$ is diamagnetic,[6a] while $\mathbf{7}^{2+}$ and $\mathbf{8}^{2+}$ are both spin transition ions, showing temperature-dependent mixtures of singlet and triplet in the solid state.[8,34] Magnetic studies will be reported separately.

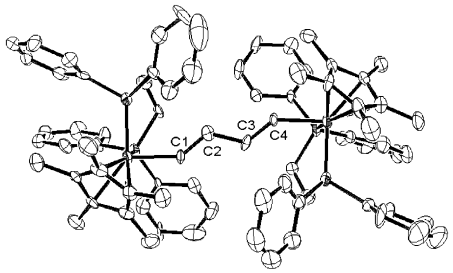

Figure 6. View of the molecular structure of **6** showing 50% thermal ellipsoids. The view is along an approximate C_2 axis, perpendicular to the bridge plane.

Conclusions

The data reported herein for **5**, **6**, and their oxidized forms, along with literature data, allow for the systematic evaluation of several structural variations in the diiron complexes: dppm vs dppe, Cp vs Cp*, butadienediyl vs butadiynediyl, and butadienediyl vs dimethoxybutadienediyl. Observed spectroscopic variations are significant and in a couple cases quite large. Nonetheless, each member of the series of bridged diiron MV cations ($\mathbf{4}^+-\mathbf{8}^+$) is observed to be a strongly coupled, delocalized ion. Where possible, explanations have been given for the observed spectral differences on the basis of simple electronic considerations or steric arguments.

The butadienediyl vs butadiynediyl (double bonds vs triple bonds) comparison in terms of coupling ability of the bridge is best made through effective coupling parameters, H_{ab}, for complexes $\mathbf{6}^+$ and $\mathbf{7}^+$. These values show that the triple bonds are slightly better at promoting electronic coupling between the iron centers in these complexes. The precise reasons for this difference are not yet clear.

Though less direct in the evaluation of electronic coupling, analysis of comproportionation constants, K_c, derived from CV ΔE values, as well as analysis of the E values themselves, have provided much insight into various effects that lead to thermodynamic stabilization or destabilization of the different cationic and dicationic species.

Experimental Section

All reactions and manipulations were carried out under a dinitrogen atmosphere unless otherwise noted. Solvents were degassed and purified by distillation under dinitrogen from appropriate drying agents (Na/benzophenone for THF; CaH_2 for toluene, benzene, pentane, and CH_2Cl_2). (Pentamethylcyclopentadienyl)iron dicarbonyl dimer was purchased from Strem Chemical Co., and *cis*-3,4-dichlorocyclobutene was obtained from Fluka Chemical Co. Ferrocenium hexafluorophosphate ($FcPF_6$) was recrystallized from ethanol. NMR spectra were recorded on a Bruker DPX-300 spectrometer. Electrochemical measurements were obtained with a BAS CV-27 potentiostat. CV samples were prepared in Bu_4NPF_6 electrolyte solution (0.1 M) in CH_2Cl_2 and performed in a three-chambered electrochemical cell, separated by two glass frits. The working electrode was a platinum disk, the auxiliary electrode was a platinum wire, and the pseudoreference electrode was a silver wire. Potentials were internally referenced to the $Cp_2Fe^{0/+}$ couple by adding Cp_2Fe at the end of the experiment. EPR spectra were obtained on a Varian E-9 EPR E-line spectrometer with variable-temperature accessories. Spectra were referenced to a solid sample of diphenylpicrylhydrazine (DPPH) standard ($g = 2.0036$ G).[35] Electronic

(33) (a) Hurst, S. K.; Cifuentes, M. P.; Morrall, J. P. L.; Lucas, N. T.; Whittall, I. R.; Humphrey, M. G.; Asselberghs, I.; Persoons, A.; Samoc, M.; Luther-Davies, B.; Willis, A. C. *Organometallics* **2001**, *20*, 4664−4675. (b) Younus, M.; Long, N. J.; Raithby, P. R.; Lewis, J.; Page, N. A.; White, A. J. P.; Williams, D. J.; Colbert, M. C. B.; Hodge, A. J.; Khan, M. S.; Parker, D. G. *J. Organomet. Chem.* **1999**, *578*, 198−209.

(34) (a) Le Narvor, N.; Lapinte, C. *C. R. Acad. Sci., Ser. IIc*: *Chim.* **1998**, *1*, 745−749 (b) Paul, F.; Lapinte, C. *Physical Organometallic Chemistry* **2002**, *3*(Unusual Structures and Physical Properties in Organometallic Chemistry), 219−295.

spectra were taken on a Shimadzu UVPC-30 spectrometer. Cuvettes fitted with vacuum stopcock closures were used to study air-sensitive samples. Elemental analyses were performed by E & R Microanalysis, Co., Parsippany, NJ.

{[Cp(dppm)Fe]2(μ-CH=CHCH=CH)}[BF4]2 (4[BF4]2). Compound **4**[6a] (23.2 mg, 22 μmol) was combined with solid silver tetrafluoroborate (9.1 mg, 48 μmol) and cooled to 0 °C. Cold CH_2Cl_2 (4 mL) was added by cannula. A vivid purple mixture resulted, and the mixture was stirred at 0 °C for 30 min and then filtered twice through Celite (3−4 in.) in air and washed through with CH_2Cl_2. Solid product was precipitated by the addition of cold pentane with stirring. Recrystallization from pentane/CH_2Cl_2 gave 8.7 mg of **4[BF4]2** (32%). ^{1}H NMR (acetone-d_6): δ 13.71 (m, 2H), 7.70−7.30 (m, 40H), 6.96 (m, 2H), 5.97 (m, 4H), 5.33 (s, 10H).^{31}P NMR (CD_2Cl_2): δ 26.8. Anal. Calcd for $C_{64}H_{58}B_2F_8Fe_2P_4$: C, 62.17; H, 4.73. Found: C, 62.11; H, 4.82.

{[Cp(dppm)Fe]2(μ-CH=CHCH=CH)}BF4 (4[BF4]). To a stirred solution of **4** (13.4 mg, 13 μmol) in CH_2Cl_2 (2 mL) at 0 °C was added a cold solution of **4[BF4]2** (15.9 mg, 13 μmol) in CH_2Cl_2 (2 mL). Stirring was continued for 30 min. Solid product was precipitated by adding cold pentane and stirring well. Yield: 12.5 mg (42%). Anal. Calcd for $C_{64}H_{58}BF_4Fe_2P_4$: C, 66.87; H, 5.09. Found: C, 66.51; H, 5.18.

{[Cp(dppm)Fe]2(μ-CH=CHCH=CH)}[PF6]2 (4[PF6]2). Compound **4** (13.1 mg, 12 μmol) in CH_2Cl_2 at 0 °C was added to $FcPF_6$ (9.7 mg, 29 μmol) in CH_2Cl_2 at 0 °C, and the mixture was stirred for 30 min. Solid product was precipitated by the addition of cold pentane with stirring. Yield: 16.3 mg (98%). The ^{1}H NMR spectrum was identical with that of **4[BF4]2**.

{[Cp(dppm)Fe]2(μ-CH=CHCH=CH)}PF6 (4[PF6]). Spectroscopic samples of **4[PF6]** were prepared by oxidation of **4** with 1 equiv $FcPF_6$ or by comproportionation of **4** and **4[PF6]2**.

[Cp(dppe)Fe]2(μ-CH=CHCH=CH)[11a] **(5).** A mixture of **1** (50.8 mg, 0.13 mmol), dppe (105 mg, 0.27 mmol), and THF (210 mL) was photolyzed under nitrogen for 40 min in a 250 mL vessel at −20 °C, using a 450 W Hanovia broad-band UV lamp in a quartz immersion well. Solvent was removed in vacuo from the brown-orange mixture. The residue was redissolved in toluene (5 mL) with a few drops of benzene. The solution was filtered through glass wool, layered with pentane (5 mL), and placed in a −25 °C freezer for 2 days. The crystals obtained were washed with pentane and dried under vacuum. Yield from two crops: 59 mg (43%). ^{1}H NMR (C_6D_6): δ 7.69−6.96 (m, 40H), 5.47 (s, 4H), 4.20 (s, 10H), 2.14 (m, 4H), 1.96 (m, 4H). ^{13}C NMR (C_6D_6): δ 154.6, 144.7 (t, J_{PC} = 15 Hz), 139.9−128.9 (Ph), 80.6, 27.7 (t, J_{PC} = 53 Hz). ^{31}P NMR (C_6D_6): δ 110.6.

{[Cp(dppe)Fe]2(μ-CH=CHCH=CH)}PF6 (5[PF6]). To a stirred solution of **5** (25 mg, 23 μmol) in CH_2Cl_2 (10 mL) at 0 °C was added dropwise $FcPF_6$ (19 μmol) in 15 mL of CH_2Cl_2. Stirring was continued for 20 min. Solid product was precipitated by adding cold pentane to the cold reaction mixture and stirring well. Yield: 22 mg (94%).

{[Cp(dppe)Fe]2(μ-CH=CHCH=CH)}[PF6]2 (5[PF6]2). To a stirred solution of **5** (18 mg, 16 μmol) in CH_2Cl_2 (10 mL) at 0 °C was added dropwise $FcPF_6$ (32 μmol) in 16 mL of CH_2Cl_2. A vivid purple mixture resulted, and stirring was continued for 20 min. Solid product was precipitated three times by the addition of pentane to a CH_2Cl_2 solution. Yield: 18 mg (82%). ^{1}H NMR (CD_2Cl_2): δ 13.09 (dd, 2H), 7.52−7.00 (m, 40H), 6.53 (dd, 2H), 4.97 (s, 10H), 3.68 (br, 4H), 3.32 (br, 4H). ^{13}C NMR (CD_2Cl_2): δ 292.7, 145.7, 137−128.9 (Ph), 93.9, 30.2 (t). The C_α signal (292.7 ppm) was obtained through HMQC. ^{31}P NMR (CD_2Cl_2): δ 101.7. Anal. Calcd for $C_{66}H_{62}F_{12}Fe_2P_6$: C, 57.41; H, 4.53. Found: C, 57.16; H, 4.48.

[Cp*(CO)2Fe]2(μ-*trans*-3,4-cyclobutenediyl) (10).[11] To a stirred THF suspension (18 mL) of (pentamethylcyclopentadienyl)iron dicarbonyl dimer (500 mg, 1.01 mmol) was added 0.5 mL (ca. 10 mmol) of 1:5 Na/K alloy. The solution color changed from dark red-brown to yellow in 5−10 min. After 30 min, the mixture was centrifuged and filtered to remove the fine alloy droplets. The THF solution of the anionic complex was stored at −25 °C in a drybox freezer. The anion was stable in THF for at least 24 h but was normally used within 2 h. To the precooled (−25 °C) anion solution was added neat *cis*-3,4-dichlorocyclobutene (50 μL, 0.54 mmol). The mixture was stirred at room temperature for 1 h, which furnished a dark brown solution. The reaction mixture was then evaporated under vacuum at room temperature to dryness, followed by extraction with pentane (5 × 20 mL). The organic phases were combined, centrifuged, filtered through a Celite pad, and cooled to −25 °C for 48 h. A precipitate was formed in the pentane solution, which was often contaminated by the iron dimer starting material; one more recrystallization in pentane was performed in order to get pure compound **10**. Yield from 2 crops: 120 mg (22%). ^{1}H NMR (C_6D_6): δ 6.35 (t, J = 0.8 Hz, 2H), 3.29 (t, J = 0.8 Hz, 2H), 1.54 (s, 30H). ^{13}C NMR (C_6D_6): δ 219.0, 138.5, 94.7, 54.0, 8.7. FTIR (KBr, cm^{-1}): 3049.6 w, 2914.5 s, 1969.2 s, 1927.0 s, 1741.3 s, 1488.1 w, 1378.4 m, 1032.4 m, 998.6 m, 846.7 w.

[Cp*(CO)2Fe]2(μ-CH=CHCH=CH)[11] **(9).** The yellow **10** (200 mg, 0.037 mmol) was dissolved in 15 mL of THF in a Pyrex vessel and heated to 65 °C for 1 h. The solution was then evaporated under vacuum at room temperature. If purification was desired (for analysis or if the sample of **10** was not completely pure), the residue was dissolved in a minimum amount of THF, onto which 4 volumes of pentane was layered. The solution was moved to a −25 °C freezer without disturbance. After 48 h, the mother liquor was removed and the solid was washed with 0.5 mL of precooled (−25 °C) pentane. Two crops gave 190 mg of compound **9** (65%). ^{1}H NMR (C_6D_6): δ 7.01 (AA′BB′, $J_{\alpha\beta}$ = 15 Hz, $J_{\beta\beta'}$ = 9 Hz, $J_{\alpha\beta'}$ = −1 Hz, 2H), 6.45 (AA′BB′, identical with 7.01 ppm pattern, 2H), 1.40 (s, 30H). ^{13}C NMR (C_6D_6): δ 220.0, 149.0, 137.9, 97.0, 9.7. FTIR (KBr, cm^{-1}): 3007.4 m, 2965.2 m, 2855.4 w, 1977.7 s, 1918.6 s, 1732.9 s, 1496.6 m, 1378.4 s, 1285.6 m, 1125.2 w, 1023.9 w, 973.3 w. Anal. Calcd for $C_{28}H_{34}Fe_2O_4$: C, 61.56; H, 6.27. Found: C, 61.25; H, 6.52.

[Cp*(dppe)Fe]2(μ-CH=CHCH=CH)[11] **(6).** A mixture of **9** (22 mg, 0.040 mmol), dppe (33 mg, 0.083 mmol), and THF (20 mL) was photolyzed for 1 h in a 25 mL Pyrex vessel at 0 °C, using a 450 W Hanovia broad-band UV lamp. During the first 10 min, the solution turned dark brown. The vessel was flushed with nitrogen and shaken three times during the photolysis. The THF solution was filtered, solvent was removed under vacuum, and the residue was redissolved in a minimum amount of pentane. The pentane solution was placed in a −25 °C freezer for 2 days. Removal of the mother liquor and rinsing with cold pentane (−25 °C) afforded large dark purple-red crystals of compound **6** (20 mg, 40%). Recrystallization from pentane gave an X-ray-quality crystal, whose crystal data showed the presence of **6** and three severely disordered molecules of pentane in the asymmetric unit. ^{1}H NMR (C_6D_6): δ 7.70 (t, J = 7 Hz, 8H), 7.36 (m, 8H), 7.20 (m, 8H), 7.12 (m, 16H), 6.03 (AA′BB′, $J_{\alpha\beta}$ = 17 Hz, $J_{\beta\beta'}$ = 7 Hz, $J_{\alpha\beta'}$ = −2 Hz, 2H), 5.46 (AA′BB′, identical with 6.03 ppm pattern, 2H), 2.70 (m, 4H), 1.98 (m, 4H), 1.43 (s, 30H). ^{13}C NMR (C_6D_6): δ 154.7, 150.9 (t, J_{PC} = 31 Hz), 142.5, 142.1, 138.7, 138.3, 135.4, 134.2, 87.3, 31.1 (d, J_{PC} = 53 Hz), 10.2. ^{31}P NMR (C_6D_6): δ 109.1. FTIR (KBr, cm^{-1}): 3051.6 m, 2961.7 m, 2916.8 m, 2871.8 m, 1599.1 m, 1575.0 w, 1508.7 s, 1478.5 w, 1430.3 m, 1291.6 w, 1243.4 s, 1177.1 m, 1086.7 m, 1032.4 m, 911.8 w, 827.4 s, 743.0 w, 694.8 s, 658.6 s, 525.9 s, 489.8 m. Anal. Calcd for $C_{76}H_{82}Fe_2P_4$: C, 74.15; H, 6.71. Found: C, 73.88; H, 6.92.

{[Cp*(dppe)Fe]2(μ-CH=CHCH=CH)}PF6 (6[PF6]). To a stirred solution of [Cp*(η2-dppe)Fe]2(μ-CH=CHCH=CH) (10 mg, 8.0 μmol) in CH_2Cl_2 (2 mL) at −25 °C was added dropwise

(35) Garstens, M. A.; Singer, L. S.; Ryan, A. H. *Phys. Rev.* **1954**, *96*, 53−56.

$FcPF_6$ (8.0 μmol) in CH_2Cl_2. The orange solution turned purple-red in a few minutes. Stirring was continued for 30 min. Solid product was precipitated, if desired, by adding cold pentane to the cold reaction mixture and stirring well. Anal. Calcd for $C_{76}H_{82}F_6Fe_2P_5$: C, 62.14; H, 5.62. Found: C, 61.98; H, 5.25.

{[Cp*(dppe)Fe]$_2$(μ-CH=CHCH=CH)}[PF$_6$]$_2$ (6[PF$_6$]$_2$). To a stirred solution of **6** (51 mg, 41 μmol) in CH_2Cl_2 (15 mL) at −78 °C was added dropwise $FcPF_6$ (82 μmol) in 10 mL of CH_2Cl_2. A vivid purple mixture resulted, and stirring was continued for 30 min. Recrystallization from pentane/CH_2Cl_2 gave 30 mg of **6[PF$_6$]$_2$** as deep blue-black crystals (48%). ^{1}H NMR (CD_2Cl_2): δ 13.98 (br, 2H), 7.4−6.7 (m, 42H), 3.75 (br, 4H), 3.31 (br, 4H), 1.10 (s, 30H). ^{13}C NMR (CD_2Cl_2): δ 262.0, 152.0, 138.1−128.9 (Ph), 107.0, 33.0, 10.2. ^{31}P NMR (CD_2Cl_2): δ 92.0. Anal. Calcd for $C_{76}H_{82}F_{12}Fe_2P_6$: C, 53.48; H, 4.84. Found: C, 53.68; H, 5.12.

X-ray Crystallography. Crystallographic data for **6** were collected with a Bruker P4 diffractometer equipped with a SMART CCD system[36] and using Mo Kα radiation (λ = 0.710 73 Å). The data were collected at 293 K and corrected for Lorentz and polarization effects.[37] Absorption corrections were made using SADABS.[38] The structure solution and refinement were carried out using the SHELXTL[39] crystallographic software package. The structure was solved using direct methods, and all of the non-hydrogen atoms were located from the initial solution. After all of the non-hydrogen atoms were located, the model was refined against F^2, initially using isotropic and then anisotropic thermal displacement parameters, until the final value of Δ/σ_{max} was less than 0.001. Crystal data for **6** are summarized in Table 6. Selected distances and angles are shown in Table 5.

Acknowledgment. We thank the donors of the Petroleum Research Fund, administered by the American Chemical Society, for support of this research, Professor Teresa Freedman for help with a DFT calculation, and Professor Claude Lapinte for helpful communications.

Supporting Information Available: Tables of crystal data, atomic coordinates, bond lengths and angles, anisotropic temperature factors, calculated hydrogen positions, and molecular views for compound **6**; these data are also available in electronic form as CIF files. This material is available free of charge via the Internet at http://pubs.acs.org.

OM0300979

(36) SMART, Data Collection Software, version 4.050; Siemens Analytical Instruments Inc., Madison, WI, 1966.

(37) SAINT, Data Reduction Software, version 4.050; Siemens Analytical Instruments, Madison, WI, 1996.

(38) Sheldrick, G. M., SADABS; University of Göttingen, Göttingen, Germany, 1996.

(39) SHELXTL PC; Siemens Analytical X-ray Instruments Inc., Madison, WI, 1993.